^{19}F and $^{1,2}H$ ENDOR Study of Distal-Pocket N(ϵ)–H···F Hydrogen Bonding in Fluorometmyoglobin

Yang-cheng Fann, Jui-lin Ong, Judith M. Nocek, and Brian M. Hoffman*

Contribution from the Department of Chemistry, 2145 Sheridan Road, Northwestern University, Evanston, Illinois 60208-3113

Received January 9, 1995[⊗]

Abstract: ^{19}F and $^{1,2}H$ continuous-wave and pulsed electron nuclear double resonance (ENDOR) measurements of fluorometmyoglobin (MbF) frozen solutions are shown to provide probes of subtle structural features at the heme that are not directly accessible through X-ray methods. Although the EPR spectrum of MbF is pH invariant, the ^{19}F data show that MbF exists in low- and high-pH forms that are related by a one-proton equilibrium with pK_a = 7.6(1). The $^{1,2}H$ ENDOR shows that F^- is hydrogen-bonded to the N(ϵ) H of distal histidine (E7) at all pH values between 5.5 and 11. The pH-dependent interconversion is assigned to deprotonation at N(δ) of the charged (imidazolium) form of His(E7). The data further gives metrical parameters for the H-bond, showing it to be relatively short with r(F···H) = 1.57(5) Å. Complete determination of the ^{19}F hyperfine tensor discloses a slight tilt of Fe–F^- (non-coaxiality of g and hyperfine tensors). The tilt is associated with the H-bond: it is 5.0(5)° in the low-pH form and 3.5(5)° in the high. The ^{19}F tensor components change slightly upon deprotonation: low pH, $A_{\|}$ = +127.0(4) MHz, $A_{\perp}$ = +64.0(4) MHz; high pH, $A_{\|}$ = +130.0(4) MHz, $A_{\perp}$ = +67.5(4) MHz. Surprisingly, there is a deuterium isotope effect on the ^{19}F coupling in the low-pH form. The signs of the hyperfine components are derived from the pseudonuclear Zeeman effect in the ^{19}F ENDOR. This effect also gives to high precision the axial zero-field splitting parameter, D, whose value is determined by the energies of excited states. D also is pH dependent: low-pH form, D = 6.1(1) cm^{-1}; high-pH form, D = 5.2(1) cm^{-1}.

Introduction

The molecular mechanisms for controlling the ligand affinities of hemoproteins have been the subject of intensive research for many decades.[1] In particular, steric and/or hydrogen bonding with the distal amino acid residues may alter affinities and cause structural perturbations of the heme, such as tilting of the exogenous ligand.[2,3] The ability to detect and characterize such interactions and to identify the participating residue is essential for understanding the mechanism whereby the heme environment regulates ligand binding affinity. The present study of horse fluorometmyoglobin (MbF) shows that ^{19}F and $^{1,2}H$ pulsed and continuous-wave (CW) electron nuclear double resonance (ENDOR) spectroscopies provide sensitive probes of distal pocket interactions.

Although electron paramagnetic resonance (EPR) and ENDOR spectroscopies have been used extensively to study electronic and structural properties of hemeproteins, ENDOR studies of frozen solutions of high-spin hemeproteins generally have been limited to spectra taken in the g-2 region of the EPR envelope[4] and no ^{19}F measurements have been reported. In this first ^{19}F ENDOR study of a fluorometmyoglobin, data collected across the whole EPR envelope show that the measurement is exceptionally sensitive to the heme environment and discloses small changes in ground-state electronic structure caused by subtle structural perturbations. Indeed, it is possible to detect a change in the relative orientations of **g** and **A** tensors by as little as ~1°. In addition, the so-called pseudonuclear Zeeman (pnZ) effect[5] observed in ^{19}F ENDOR provides high-precision data about excited states, through determinations of zero-field splitting (ZFS) parameters.

EPR spectra of MbF are pH invariant, but ^{19}F ENDOR measurements at different pH values show that MbF exists in two forms that are related by a protonation–deprotonation equilibrium with pK_a = 7.6(1). $^{1,2}H$ ENDOR measurements show that the N(ϵ) H of the distal histidine residue (E7) is hydrogen-bonded to the F^- ligand at all pH values; the pH-dependent interconversion involves the deprotonation at N(δ) of the low-pH, imidazolium form of the histidine. Analysis discloses a short F···H bond, with a bond length of r ~1.57(5) Å, whose presence appears to greatly stabilize the bound F^-. Overall, the $^{1,2}H$ and ^{19}F ENDOR measurements of fluoro-hemoproteins are sensitive to subtle structural features at the heme that are likely to be inaccessible to X-ray methods.

Procedure and Theory

Proteins. Horse ferric myoglobin (Mb^+) was obtained from Sigma Chemical Co. Lyophilized powder was dissolved in 50 mM potassium phosphate buffer at pH 6. To ensure complete oxidation, 1–2 equiv of potassium ferricyanide was reacted with the protein solution. After about 1 h, the protein solution was washed using microconcentrators with several volumes of working buffer to remove unreacted ferricyanide. Fluorometmyoglobin (MbF) was prepared by diluting the protein solution with 0.2 M potassium fluoride buffered to the desired pH and concentrated to greater than 2 mM with Centricon microconcentrators. All aqueous buffers contained 60% (v/v) glycerol, and the pH values for all buffered solutions described in this work were recorded as read from the pH meter. Samples

[⊗] Abstract published in *Advance ACS Abstracts,* May 15, 1995.

(1) (a) Antonini, E.; Brunori, M. *Hemoglobin and Myoglobin in their Reactions with Ligands*; American Elsevier Publishing Co.: New York, 1971. (b) Springer, B. A.; Sligar, S. G.; Olsen, J. S.; Phillips, G. N., Jr. *Chem. Rev.* **1994**, *94*, 699.

(2) Phillips, S. E.; Schoenborn, B. P. *Nature* **1981**, *292*, 81.

(3) Lecomte, L. T. J.; LaMar, G. N. *J. Am. Chem. Soc.* **1987**, *109*, 7219–7220.

(4) (a) Scholes, C. P.; Isaacson, R. A.; Feher, G. *Biochim. Biophys. Acta* **1972**, *263*, 448–452. (b) Feher, G.; Isaacson, R. A.; Scholes, C. P.; Nagel, R. *Ann. N.Y. Acad. Sci.* **1973**, *222*, 86–101.

(5) Abragam, A.; Bleaney, B. *Electron Paramagnetic Resonance of Transition Ions*, 2nd ed.; Claren Press: Oxford, 1970.

0002-7863/95/1517-6109$09.00/0

in D_2O (99.9 atom % D, Isotec) contained 60% (v/v) glycerol-$(OD)_3$ (98 atom % D, from Aldrich).

Sample concentrations were determined using $\epsilon_{408}(Mb^+)$ = 188 mM^{-1} cm^{-1} and $\epsilon_{408}(MbF)$ = 146 mM^{-1} cm^{-1} with a Hewlett-Packard diode array spectrophotometer.[1]

ENDOR Measurements. CW ENDOR spectra were recorded with a Varian associates E109 EPR spectrometer equipped with an E110 35 GHz microwave bridge using 100 kHz field modulation as described previously.[6] Pulsed ENDOR spectra were obtained on a locally-built spectrometer operating at X band (~9.5 GHz).[7] All ^{19}F pulsed ENDORspectra were recorded using a Davies pulse sequence $(\pi-\pi/2-\pi)$[8] with π pulse width, 40 ns; short RF pulse widths (≈3.5 μs) maximized ENDOR responses.

Theory. The spin Hamiltonian used to describe EPR and ENDOR transitions for a high-spin Fe^{3+} ($S = {}^5/_2$) interacting with a single $I = {}^1/_2$ nucleus is given by eq 1,[5] where g_e and g_N

$$H = g_e\beta\mathbf{B}\cdot\mathbf{S} - g_N\beta_N\mathbf{B}\cdot\mathbf{I} + \mathbf{S}\cdot\mathbf{A}\cdot\mathbf{I} + \mathbf{S}\cdot\mathbf{D}\cdot\mathbf{S} \qquad (1)$$

are electronic and nuclear g factors, β and β_N are Bohr and nuclear magnetons, and **B** is the applied magnetic field. **S** and **I** refer to electron and nuclear spins, and **A** is the hyperfine tensor. **D** is the zero-field splitting (ZFS) tensor, characterized by the axial and rhombic ZFS parameters (D and E) that split the $2S + 1 = 6$ levels into three Kramers doublets with $m_s = \pm{}^1/_2$ being the lowest, corresponding to $D > 0$. The $m_s = \pm{}^1/_2$ doublet in a $S = {}^5/_2$ spin system can be treated as an effective $S' = {}^1/_2$ system described by the effective spin Hamiltonian

$$H' = \beta\mathbf{S}'\cdot\mathbf{g}'\cdot\mathbf{B} + \beta_N\mathbf{I}\cdot\mathbf{g}^N\cdot\mathbf{B} + \mathbf{S}'\cdot\mathbf{A}'\cdot\mathbf{I} \qquad (2)$$

where $\mathbf{g}'$ and $\mathbf{A}'$ are the orientation-dependent **g** and hyperfine tensors in the effective spin representation. For MbF, the ZFS tensor is axial, with $E = 0$, in which case g' is axial with $g_{\parallel} = g_e$, $g_{\perp} \cong 3g_e \approx 6$. The hyperfine tensor in the effective-spin representation is given by $\mathbf{A}' = \mathbf{A}\cdot(\mathbf{g}'/g_e)$. Mixing of the $m_s = \pm{}^3/_2$ doublet into the ground-state doublet by the joint influence of the electron Zeeman and electron–nuclear hyperfine interaction causes the nuclear Zeeman interaction to assume a tensor form; $\mathbf{g}^N$ is an effective nuclear **g** tensor which is coaxial with the zero-field splitting tensor (**D**).[5]

The samples employed in the study were frozen solutions with a random distribution of all possible protein orientations, but the principal values of the hyperfine tensor and its orientation relative to the **g**′-tensor axis (the ZFS axis) can be determined by simulating a set of ENDOR spectra recorded at g values (or fields) across the EPR spectrum. The theory and practice of such orientation-selective ENDOR for frozen solutions has been described in detail elsewhere,[9,10] as has the program used to simulate all ENDOR spectra described in this work.[11] This program calculates ENDOR frequencies to determine the hyperfine tensor, $\mathbf{A}'$ ($S' = {}^1/_2$ representation), and quadrupole terms where appropriate, and their relative orientation to the **g** tensor. As described below, ^{19}F spectra at $g_{\parallel} = 2$ and $g_{\perp}' = 6$ also were calculated by exact diagonalization of eq 1 to allow precise determination of the ZFS parameter, D.

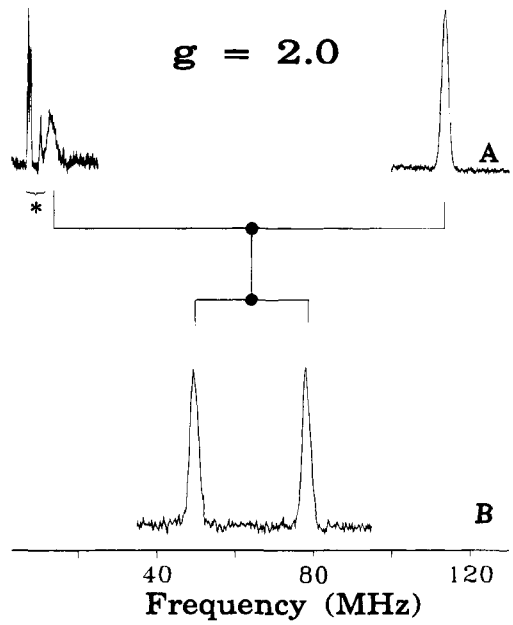

Figure 1. ^{19}F ENDOR spectra of ferrimyoglobin fluoride taken at g = 2 in pH = 6.0 buffer solution. (A) 34.96 GHz CW ENDOR spectra showing both ν_+ and ν_- branches of ^{19}F ENDOR transitions which is indicated by the "goal post" symbol; $A(^{19}F)/2$ is also shown as (●). Conditions: magnetic field (B_0), 12489 G; microwave power, 1 mW; modulation amplitude, 1.0 G; RF scan rate, 2 MHz/s, 25 scans; 2 K. (B) 9.369 GHz Davies pulsed ^{19}F ENDOR spectrum. Conditions: B_0, 3347 G; $\pi/2$ microwave pulse width, 20 ns; τ_{12}, 10.14 μs; τ_{23}, 202 ns; RF pulse width, 3.5 μs; repetition rate, 100 Hz; samplings per data point, 30; 256 data points per spectrum; temperature, 2 K. * represents the ν_+ branches of ^{14}N resonances.

Results and Discussion

EPR. The EPR spectrum of frozen-solution high-spin MbF at 2 K is characterized by an axial signal with $g_{\parallel} = 2$ and $g'_{\perp} = 6$, where the direction of the $g_{\parallel} = 2$ axis is closely aligned with the normal to the heme plane.[12] It shows a resolved ^{19}F hyperfine splitting of about 46 G (~129 MHz) at $g_{\parallel} = 2$. Whereas Kotani and Morimoto detected slight rhombicity in the EPR spectrum of a single crystal of MbF,[13] this effect is not seen in the frozen-solution EPR spectrum presumably due at least in part to large inhomogeneous EPR line broadening.[14] In the process of simulating ENDOR spectra, discussed below, we tested whether inclusion of an unresolved rhombicity in **g** would modify any of the results or conclusions. It was found that the reported rhombicity ($g_x = 5.87$, $g_y = 5.98$) could have no influence on the present study.

^{19}F ENDOR. The 35 GHz CW ENDOR spectrum of MbF at pH = 6.0 taken at $g_{\parallel} = 2$ (Figure 1A) shows ^{19}F peaks at 114 and 13 MHz. These are denoted as ν_+ and ν_- transitions and are centered at $A'_{\parallel}(^{19}F)/2 = 63.5$ MHz ($A'_{\parallel}(^{19}F) = 127$ MHz) and split by a value close to twice its Larmor frequency. To the first order, $\nu_{\pm} = |A'/2 \pm \nu(^{19}F)|$ and $\nu(^{19}F) = 50.3$ MHz; we return below to the fact that $\delta\nu_{\pm} = \nu_+ - \nu_-$ differs significantly from $2\nu(^{19}F)$. This assignment was confirmed by

(6) Werst, M. M.; Davoust, C. E.; Hoffman, B. M. *J. Am. Chem. Soc.* **1991**, *113* (5), 1533–1538.
(7) Fan, C.; Doan, P. E.; Davoust, C. E.; Hoffman, B. M. *J. Magn. Reson.* **1992**, *98*, 62–72.
(8) Davies, E. R. *Phys. Lett.* **1974**, *47A*, 1.
(9) Hoffman, B. M.; DeRose, V. J.; Doan, P. E.; Gurbiel, R. J.; Houseman, A. L. P.; Telser, J. *Biological Magnetic Resonance, Vol. 13: EMR of Paramagnetic Molecules*; Berliner, L. J., Reuben, J., Eds.; Plenum Press: New York, 1993.
(10) Gurbiel, R. J.; Fann, Y. C.; Surerus, K. K.; Werst, M. M.; Musser, S. M.; Doan, P. E.; Chan, S. I.; Fee, A. F.; Hoffman, B. M. *J. Am. Chem. Soc.* **1993**, *115*, 10888–10894.
(11) (a) The GENDOR simulation program, based on the first-order perturbation treatment of the spin Hamiltonian with an option to use a formula derived by Muha for $I = 1$, can be obtained upon requested from the authors. (b) Muha, G. M. *J. Magn. Reson.* **1982**, *49*, 431.
(12) Scholes, C. P.; Lapidot, A.; Mascarenhas, R.; Inubushi, T.; Isaacson, R. A.; Feher, G. *J. Am. Chem. Soc.* **1982**, *104*, 2724–2735.
(13) Kotani, M.; Morimoto, H. *Biochim. Biophys. Acta* **1966**, *126*, 176.
(14) Kotani, M.; Morimoto, H. *Magnetic Resonance in Biological Systems;* Pergamon Press: New York, 1967.

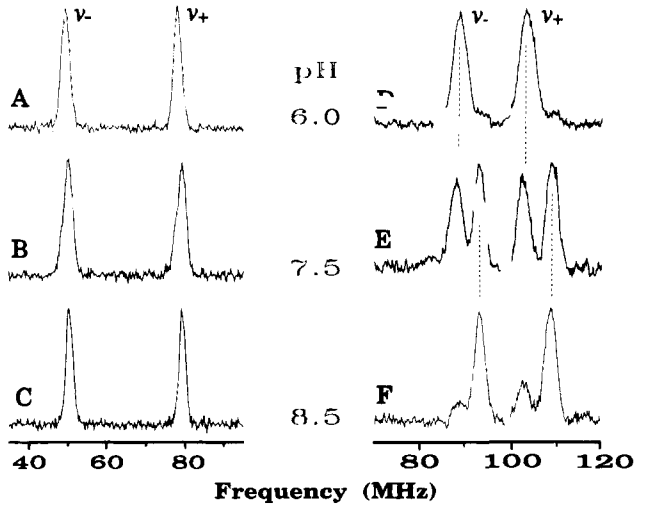

Figure 2. ^{19}F X-band pulse ENDOR spectra at $g = 2$ (A−C) and 6 (D−F) for MbF in three different pH buffers. Conditions: Davies pulse sequence with $\pi/2$ microwave pulse width = 20 ns; τ_{12}, 10.14 μs; RF pulse width, 3.5 μs; repetition rate, 100 Hz; samplings per data point, 30; 256 data points per spectrum; temperature, 2 K. (A) pH = 6, 9.369 GHz, $\mathbf{B}_0$ = 3347 G, τ_{23} = 202 ns, six scans. (B) pH = 7.5, 9.439 GHz, $\mathbf{B}_0$ = 3372 G, τ_{23} = 210 ns, 11 scans. (C) pH = 8.5, 9.378 GHz, $\mathbf{B}_0$ = 3350 G, τ_{23} = 210 ns, 10 scans. (D) pH = 6.0, 9.369 GHz, $\mathbf{B}_0$ = 1116 G, τ_{23} = 182 ns, 15 scans. (E) pH = 7.5, 9.439 GHz, $\mathbf{B}_0$ = 1124 G, τ_{23} = 178 ns, 24 scans. (F) pH = 8.5, 9.378 GHz, $\mathbf{B}_0$ = 1117 GHz, τ_{23} = 194 ns, 25 scans.

an X-band pulsed ENDOR spectrum taken at the same g value (Figure 1B), which again shows a doublet centered at $A'_{\|}(^{19}\text{F})/2 = 63.5$ MHz, but now split by close to (but not exactly) twice the ^{19}F Larmor frequency at X band, $\nu(^{19}\text{F}) = 13.5$ MHz.

The EPR spectrum of MbF, including the ^{19}F splitting at $g = 2$, as well as the ^{19}F ENDOR spectrum at $g = 2$, is independent of pH between pH = 6 and 9 (Figure 2A−C). However, ^{19}F splittings are seen in the frozen-solution EPR spectrum only at $g = 2$, whereas ^{19}F ENDOR can be collected at all fields within the EPR envelope and the spectra at other g values show surprising changes with pH. The X-band ^{19}F ENDOR spectrum recorded at $g'_{\perp} = 6$ for the pH = 6.0 MbF solution (Figure 2D) exhibits a $\nu_{\pm}$ doublet centered at 95.5 MHz, corresponding to $A'_{\perp} = 191$ MHz and split by the much smaller nuclear Zeeman interaction at $g' = 6$. Note, however, in this spectrum, there is a barely detected doublet (Figure 2D) that is ~5% as intense as the major one; it is centered at a slightly higher frequency, 101 MHz, and thus has a slightly larger hyperfine coupling ($A'_{\perp} = 202$ MHz).

This minority signal is not sample dependent; measurements on several independent samples yielded the same ENDOR pattern. Instead, a pH titration shows that these two signals are associated with two forms of MbF related by an acid/base equilibrium. As the pH of the protein solution is raised, the ^{19}F ENDOR intensity (I) at $g' = 6$ of the $A'_{\perp} = 191$ MHz form, denoted as the l form, decreases and that of the $A'_{\perp} = 202$ MHz form, denoted the h form, increases; their sum remains constant. At pH = 7.5, $I(\text{l}) \approx I(\text{h})$, and by pH = 8.5, $I(\text{l}) \gg I(\text{h})$. This effect is not observable either in the EPR spectrum or in ENDOR at $g = 2$. Figure 3 plots the pH dependence of the intensities of the low (l) and high (h) pH components of the ^{19}F ENDOR signals measured at $g' = 6$, along with independent fits of I(l) and I(h) to a function describing a single proton acid/base equilibrium. Both fits correspond to pK_a = 7.6(1), the pH where the two forms have equal intensity and where each curve has an inflection point. Clearly there is a

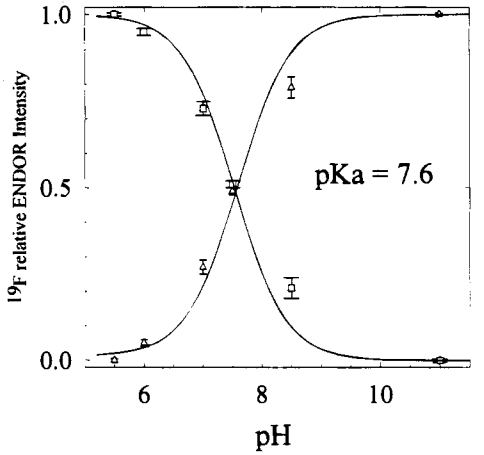

Figure 3. Relative intensity of $g' = 6$ X-band pulsed ^{19}F ENDOR peaks from low- and high-pH forms as a function of solution pH. (□) and (△) are experimental values for pH = 6 and pH = 8.5, respectively. Solid lines are curves for one proton titration with pK_a = 7.6(1).

Table 1. ^{19}F Hyperfine Coupling Tensors of Fluoride Ligand in Different pH Buffers[a]

	$A_{\|\|}$ (MHz)	$A_{\perp}$ (MHz)	θ[b]
	Aqueous Buffer		
low pH	+127.0	+64.0	5.0
high pH	+130.0	+67.5	3.5
	Deuterated Buffer		
low pH	+127.6	+65.2	5.0
high pH	+130.0	+67.5	3.5

[a] The $S = {}^5/_2$, true-spin representation. Uncertainty: A, ±0.4 MHz; θ, ±0.5°. [b] θ is defined as an Euler angle between g_z and $A_{\|\|}$ axes.

titratable proton in the vicinity of heme active site that affects the ^{19}F ENDOR signals. This is discussed in the ^{1,2}H ENDOR section.

^{19}F Hyperfine Tensors. To determine the full hyperfine tensor of the fluoride ligand in both l and h forms, we collected ENDOR spectra across the EPR envelope of each. For a $S' = {}^1/_2$ system with axial $\mathbf{g}'$ tensor, $g'_{\perp} = 6$, $g_{\|} = 2$, and axial $\mathbf{A}'(^{19}\text{F})$ tensor (with $A'_{\|}$, $A'_{\perp} \gg \nu_N$ at all fields), when the two tensors are coaxial, the ^{19}F ENDOR should exhibit a single Larmor split doublet at all fields, $g'_{\perp} \geq g'_{\text{obs}} \geq g_{\|}$ (assume $g'_{\perp} > g_{\|}$). In particular, the existence of a single doublet at $g'_{\perp}$ for a given form shows that the ^{19}F tensor very closely approximates to the stated conditions. However, although both l and h forms show a single doublet at both $g'_{\perp}$ and $g_{\|}$, this is *not* so at intermediate g' values. For the low-pH form (pH = 6), as g'_{obs} is increased from $g = 2$, the ν_+ branch of the ^{19}F signal broadens and splits into two peaks at $g' = 2.1$; the splitting increases as the field is lowered, and by $g' = 2.75$, it reaches a maximum of about 5.5 MHz. As the field is decreased further, the split peaks gradually recombine to give a broad peak that sharpens as g'_{obs} approaches $g'_{\perp}$. Similar behavior was observed in the high pH form (pH = 8.5) with a maximum splitting of about 4 MHz at $g' = 2.75$. These splittings indicate that the hyperfine and $\mathbf{g}'$ tensors are not coaxial for either the low- or high-pH form. For both forms, the full hyperfine tensor, $\mathbf{A}(^{19}\text{F})$, including the relative orientation (Table 1) with respect to $\mathbf{g}'$ (the ZFS axis system), was obtained by simulating the field-dependent ENDOR spectra across the EPR envelope. Figure 4 shows the experimental and simulated peak positions of the ν_+ branch ^{19}F ENDOR spectra taken at 35 GHz for both low- and high-pH forms of MbF. The hyperfine tensor for the low-pH sample has principal values $A_{\|} = +127$ MHz and $A_{\perp} = +64$ MHz[15] (signs are discussed below), with $A_{\|}$ having a 5° "tilt" off the principal g_z axis. For the high-pH sample, both $A_{\|}$ and

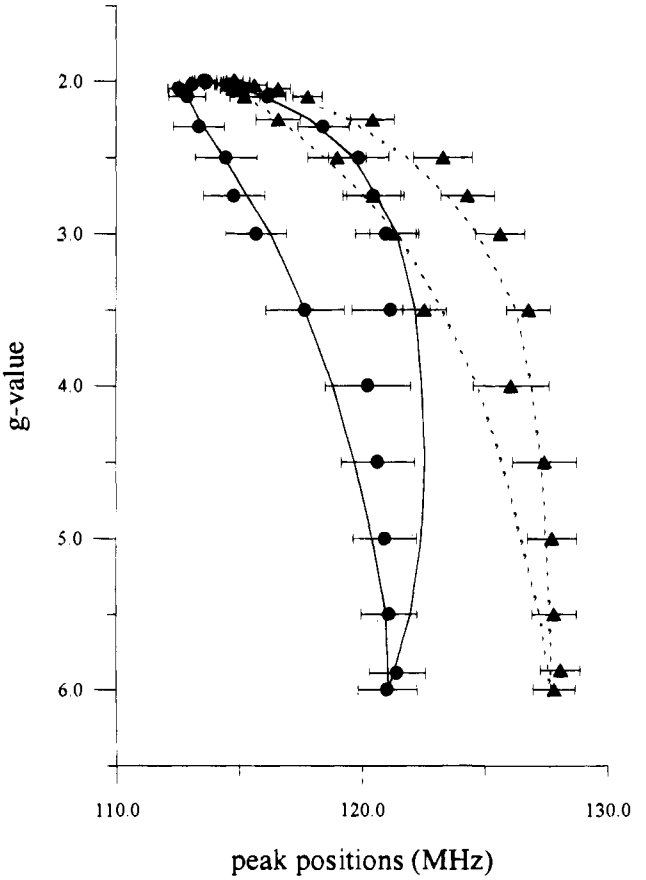

Figure 4. Plot of 35 GHz CW $\nu_+(^{19}F)$ ENDOR peak positions versus g value for low pH (●) and high pH (▲) forms. The half-height-full-width for each resolved peak is indicated as |—|. The theoretical curves for predicted peaks, calculated using ^{19}F hyperfine coupling constants listed in the Table 1, are presented as solid lines for low pH and dotted lines for high pH.

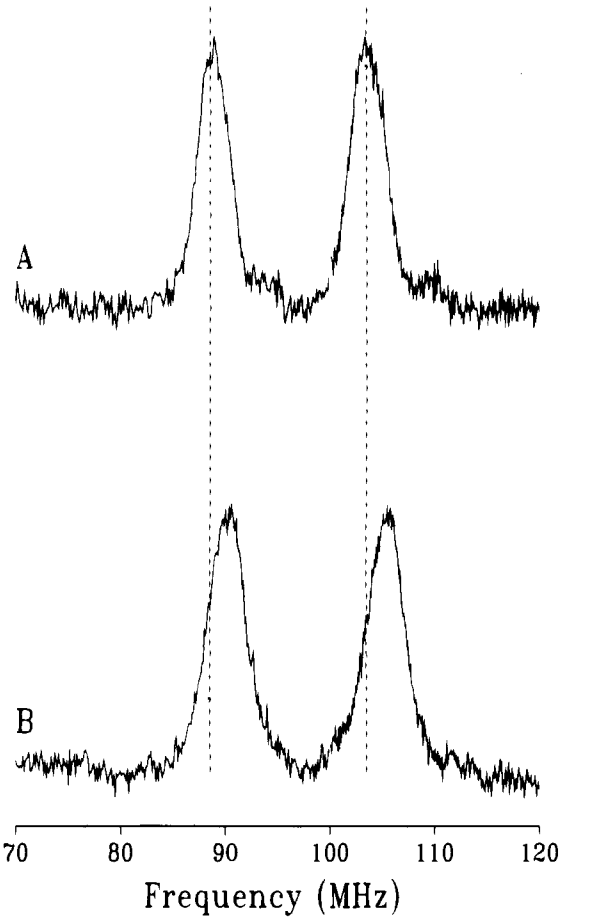

Figure 5. ^{19}F X-band pulsed ENDOR spectra of MbF in both aqueous and deuterated buffers taken at $g = 6$. Conditions: (A) same as in Figure 3D. (B) 9.536 GHz Davies pulse sequence with $\pi/2$ microwave pulse width = 20 ns; τ_{12}, 10.14 μs; τ_{23}, 174 ns; $\mathbf{B}_0$, 1136 G, RF pulse width, 3.5 μs; repetition rate, 100 Hz; samplings per data point, 30; 256 data points per spectrum; temperature, 2 K.

$A_\perp$ are increased slightly (Table 1) and the tilt angle is smaller, 3.5°; the precision in the fits of ±0.5° makes the difference in tilt angle significant. At intermediate values of pH (e.g., pH = 7.5), the ^{19}F ENDOR spectrum at a given field is essentially the weighted sum of the individual low- and high-pH spectra (data not shown). Futhermore, though slight rhombicity in the EPR spectrum has been observed in the single crystal study,[13] there is no observable change in the hyperfine couplings (A') when $g > g_\perp$ in the frozen solution samples of this study.

H/D Isotope Effect on A(^{19}F). Figure 5 shows the ^{19}F ENDOR spectra of l form MbF taken at $g'_\perp = 6$ in pH = 6 aqueous buffer (Figure 5A) and in D_2O solution (Figure 5B). The ^{19}F ENDOR pattern taken at $g'_\perp = 6$ in the D_2O buffer shows that the center of the ν_+,ν_- doublet shifts approximately 2 MHz toward higher frequency (from $A'_\perp = 192.3$ to $A'_\perp = 195.8$ MHz) compared to the same doublet in H_2O buffer. However, the field-dependent ^{19}F ENDOR of the deuterated sample shows no apparent change in the 5° tilt angle between $\mathbf{g}'$ and $\mathbf{A}'$ tensors. In contrast, ^{19}F ENDOR spectra of the high-pH form taken at $g' = 6$ show no detectable difference in either hyperfine couplings or tilt angles for H_2O and D_2O solutions. We assign this deuterium isotope effect to an influence of the titratable proton on the Fe—F bond.

(15) The ^{19}F hyperfine tensor values agree satisfactorily with those obtained from the single-crystal EPR study of sperm whale MbF, A(^{19}F) = (60.2, 66, 120) MHz.[13] However, with the lower resolution of EPR, it was not possible to detecte the non-coaxiality of **g** and **A**, the pH transition was not observed, and it is in principle not possible to learn about the ZFS parameter, D.

Sign of A and Magnitude of D. In the case of a Kramers doublet that is well-separated from all other doublets, the $\nu_\pm$ branches in an ^{19}F ENDOR spectrum are expected to be separated by twice the Larmor frequency ($2\nu^0(^{19}F)$). However, as noted above, for MbF, the splitting ($\delta\nu_\pm$) between the ν_+ and ν_- branches in the ^{19}F ENDOR is larger than $2\nu^0(^{19}F)$, with the discrepancy becoming more pronounced at $g'_\perp$. This discrepancy is the result of the pseudonuclear Zeeman (pnZ) effect, which arises because of a coupling between $m_s = \pm 1/2$ and $m_s = \pm 3/2$ doublets in second (and higher) order, through cross terms involving both electron—Zeeman and electron—nuclear hyperfine terms in eq 2.[5] The effect is commonly accounted for in the spin Hamiltonian by treating the nuclear Zeeman interaction as being controlled by a nuclear $\mathbf{g}^F$ tensor. In the case here, with an axial hyperfine interaction, the $\mathbf{g}^F$ tensor is axial with $g^F_{||}$ and $g^F_\perp$ corresponding to directions parallel and perpendicular to the unique ZFS axis, respectively. Table 2 presents the values of $g^F_{||}$ and $g^F_\perp$ for the h and l forms of MbF as determined from $\delta\nu_\pm$ at $g = g_{||}$ and $g_\perp$, respectively; the deviations of $g^F_{||}/g_F$ and $g^F_\perp/g_F$ from unity, where g_F is the intrinsic value, represent the pnZ effect.

Second-order expressions for $g^F_{||}$ and $g^F_\perp$ are readily obtained and show that $g^F_{||} = g_F$ and $g^F_\perp = g_F[1 + 4(g_e\beta_e/g_F\beta_N)(A_\perp/D)]$. The magnitude of $A_\perp$ is known from the simulations described above, and the sign of D, namely $D > 0$, is known because the $m_s = \pm 1/2$ doublet is the ground state. Thus, the analysis of the pnZ effect gives the *signs* of the components of **A** and the *value* for D; for example, the result that $g^F_{||}, g^F_\perp/g_F > 1$ requires

Table 2. Effective Nuclear g Values and Zero-Field Splitting Parameter (D) for the ^{19}F Ligand in Various pHs of Aqueous and Deuterated Buffers[a]

	$g^F_{\|}$[b]	$(g^F_{\|}/g_F)$	$g^F_{\perp}$	$(g^F_{\perp}/g_F)$	D (cm^{-1})
		Aqueous Buffer			
low pH	5.64	(1.07)	8.60	(1.64)	6.1
high pH	5.68	(1.08)	9.28	(1.77)	5.2
		Deuterated Buffer			
low pH	5.64	(1.07)	8.7	(1.66)	5.9
high pH	5.68	(1.08)	9.4	(1.79)	5.0

[a] Uncertainty: g^F ±0.05; D, ±0.1 cm^{-1}. [b] Effective nuclear g values are obtained from $\nu_+ - \nu_- = g^F\beta_N B$ where ν_+ and ν_- are measured from experimental ENDOR transitions.

that $A^F_{\|}A^F_{\perp} > 0$. As examples of the use of this effect, Scholes *et al.* used the pnZ effect in ^{57}Fe ENDOR of aquometmyoglobin[16] to determine the sign of the ^{57}Fe hyperfine couplings and we used it in ^{57}Fe ENDOR of the nitrogenase MoFe proteins to determine such signs and the value of D for the $S = {}^3/_2$ FeMo cofactor.[17]

In the present case, however, the second-order treatment is not adequate for quantitative purpose; for example, it predicts $g^F_{\|} = g_F$, contrary to observation. Instead we used exact numerical diagonalization of the full 12 × 12 spin-Hamiltonian matrix for an $S = {}^5/_2$ system interacting with ^{19}F ($I = {}^1/_2$), while varying the hyperfine and ZFS parameter, D, so as to match the calculated and experimental ν_+ *and* ν_- ENDOR transitions. These calculations permitted us to refine the magnitudes of the hyperfine tensor components, to establish the signs of both $A^F_{\|}$ and $A^F_{\perp}$, and to use ^{19}F ENDOR to directly determine D with high precision in both h and l forms of MbF at pH values between 5.5 and 11. Table 1 contains the refined hyperfine couplings with the positive sign as determined; note that the simulation of the field-dependent ^{19}F ENDOR spectra independently shows that $A_{\|}(^{19}F)$ and $A_{\perp}(^{19}F)$ have the same sign. As seen in Table 2, $D \cong 6.0(1)$ cm^{-1} in the low-pH form and D decreases by ~15% upon conversion of MbF to the high-pH form.

Spin Density on F$^-$. Although the ^{19}F of MbF has very large hyperfine coupling constants compared to those seen for most nonmetallic nuclei in biomolecules, the net spin density on ^{19}F in fact is relatively small. We can decompose the intrinsic ($S = {}^5/_2$) hyperfine tensor, $\mathbf{A}(^{19}F)$ (Table 1), into isotropic and anisotropic contributions, $\mathbf{A} = (a\mathbf{I} + \mathbf{T})$, where $\mathbf{I}$ is the unit matrix and trace $(\mathbf{T}) = 0$. The intrinsic ^{19}F isotropic hyperfine coupling constant is $a = 85$ MHz for the low-pH MbF sample and $a = 88$ MHz, ~3% greater, for the high-pH one. The observed a is related to the spin density in the 2s orbital on fluorine (ϱ^s) by the relation $a = (a_0\varrho^s/2S)$, where $S = {}^5/_2$ and $a_0(F) = 52\,870$ MHz is the value for the unit spin density.[18] This expression gives a net spin density in the 2s orbital of fluorine of $\varrho^s \sim 0.01$ in either form, with ϱ^s being 3% greater in the h form. The anisotropic contribution to the ^{19}F hyperfine tensor is dipolar in character, $T = (-t, -t, 2t)$, with $t = 21$ MHz for *both* low- and high-pH forms. This tensor itself has two contributions, one from the through-space dipolar coupling to spin localized on the Fe^{3+}, t_{Fe}, and the other from spin in the $2p_z$ orbital on F, t_F:

$$t = t_{Fe} + t_F$$

$$t_{Fe} = (g_F\beta_N g_e\beta_e/d^3)\varrho_{Fe}$$

$$t_F = t_0(F)\varrho^p/2S \qquad (3)$$

In the expression for t_{Fe}, d is the Fe−F distance, ϱ_{Fe} is the fraction of the total odd electron density on Fe, and the other symbols have the usual meanings; in that for t_F, $t_0(F) = 1760$ MHz is the coupling for one electron in $2p_z(F)$ and ϱ^p, the actual spin density in $2p_z(F)$. Taking the Fe−F bond distance as $d = 2.0$Å[19] and the spin density (ϱ_{Fe}) on Fe^{3+} as 70%,[12] we calculate $t_{Fe} = 10.8$ MHz. With $t = 21$ MHz, this gives $t_F = 10$ MHz, from which we then compute $\varrho^p \sim 0.03$ as the net spin in the $2p_z$ orbital of ^{19}F. This spin arises from bonding between the d_z^2 orbital on Fe and an s−p hybrid on F, where the p/s ratio is given by $\varrho^p/\varrho^s \approx 3/1$; that is, the contribution of F^- to the d_z^2 orbital must have the following form:

$$\Psi(d_z^2) = c_{Fe}\phi_{d_{z^2}}(Fe) - c_F[{}^1/_2(\phi^F{}_{2s} + \sqrt{3}\phi^F{}_{2p_z})] + \ldots \qquad (4)$$

where $|c_F|^2 \approx 0.04$. Clearly, even though the spin density on the fluoride ligand is small (~4%), nevertheless subtle changes in the spin distribution lead to a significant change in the hyperfine coupling constant because the intrinsic hyperfine coupling is so large. Hence, ^{19}F is a sensitive probe of the heme active site. The difference in ^{19}F couplings between h and l forms corresponds to a small increase in $|c_F|^2$ in the high-pH form, presumably reflecting an improved Fe−F bonding upon loss of the proton with $pK_a = 7.6(1)$.

Interpretation of Zero-Field Splitting. The ZFS term in eq 1 lifts the 6-fold degeneracy of the $S = {}^5/_2$ ($^6A_1$) ground state of a high-spin ferriheme. This term arises because of mixing with two higher levels of Fe^{3+} ($^4A'_2$ and $^4E'$) through the action of spin−orbit coupling in the nonspherically symmetric coordination environment of MbF.[14] Several techniques have been applied to determine zero-field splitting parameters (D values) of fluorometmyoglobin, for example, far-infrared magnetic resonance,[20] magnetic susceptibility,[21] temperature-dependent spin−lattice relaxation rate,[22] and single crystal EPR.[23] The reported values of D for fluorometmyoglobin range from 6 to 8 cm^{-1} depending on the technique used. As determined here, the low-pH sample has a value of $D = 6.1(1)$ cm^{-1}, which is much more accurate but comparable to those reported previously; the high-pH form has a significantly lower (~15%) D value. There may be a deuterium isotope dependence of D, as well as for the ^{19}F hyperfine values in the low-pH form, but any such effect is at the limit of accuracy.

One can describe D with crystal field expressions that depend on the splitting between the five d orbitals, with the key parameter being the tetragonal splitting of the t_{2g} orbitals, $\delta\epsilon_t = \epsilon_{xz,yz} - \epsilon_{xy}$. A positive D arises when $\delta\epsilon_t > 0$, which occurs when the crystal-field strength along the z direction, corresponding to the heme normal, is greater than that perpendicular to z ("axial compression").[14] The ~15% reduced value of D in the high pH form implies a roughly comparable reduction in $\delta\epsilon_t$. This change could of course come about by a simple weakening of the Fe−F interaction, with Fe−N interactions unaffected. However, $a(^{19}F)$ *increases* by ~3% in the high-

(16) Scholes, C. P.; Isaacson, R. A.; Yonetani, T.; Feher, G. *Biochim. Biophys. Acta* **1973**, *322*, 457.
(17) Venters, R. A.; Nelson, M. J.; Mclean, P. A.; True, A. E.; Levy, M. A.; Hoffman, B. M.; Orme-Johnson, W. H. *J. Am. Chem. Soc.* **1986**, *108*, 3487.
(18) Morton, J. R.; Preston, K. F. *J. Magn. Reson.* **1978**, *30*, 577−582.
(19) Edwards, S. L.; Poulos, T. L.; Kraut, J. *J. Biol. Chem.* **1984**, *259*, 12984.
(20) Brackett, G. C.; Richards, P. L. *J. Chem. Phys.* **1971**, *54*, 4383.
(21) Uenoyama, H.; Huzka, T.; Morimoto, H.; Kotani, M. *Biochim. Biophys. Acta* **1968**, *160*, 159.
(22) Scholes, C. P.; Isaacson, R. A.; Feher, G. *Biochim. Biophys. Acta* **1971**, *244*, 206.
(23) Slade, E. F.; Farrow, R. H. *Biochim. Biophys. Acta* **1972**, *278*, 450.

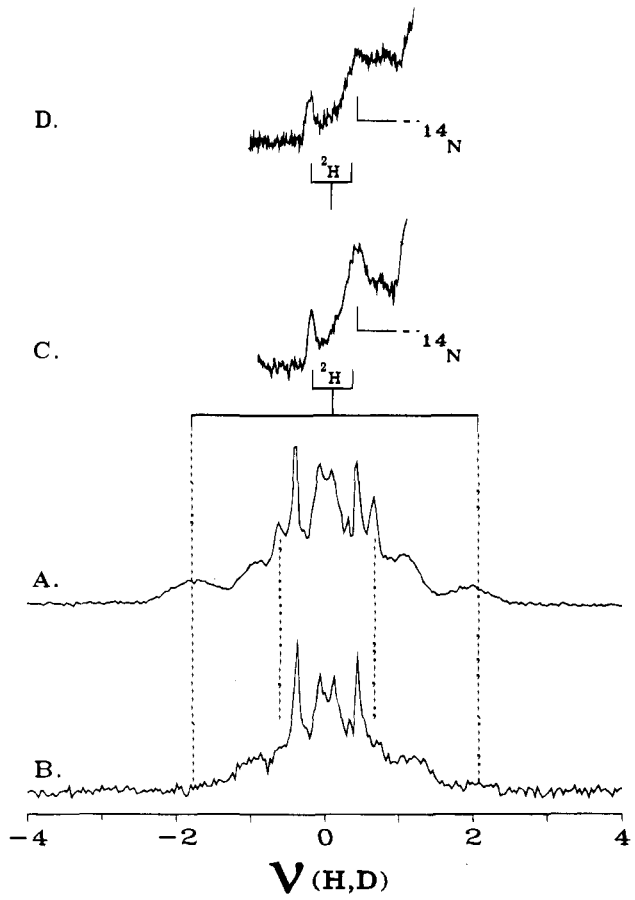

Figure 6. ^{1}H and ^{2}H X-band Mims pulsed ENDOR spectra of fluorometmyoglobin taken at $g = 2$ in both aqueous and deuterated buffers. For comparison, spectra are plotted as $\delta\nu = \nu - \nu_{(H,D)}$. Conditions: (A) ^{1}H ENDOR spectrum in aqueous pH = 6.0 solution, 9.369 GHz; $\pi/2$ microwave pulse width, 16 ns; $\mathbf{B}_0$, 3360 G; τ_{12}, 148 ns; τ_{23}, 26.62 μs; RF pulse width, 20 μs; repetition rate, 100 Hz; samplings per data point, 30; 256 data points per spectrum, 30 scans; 2 K. (B) ^{1}H ENDOR spectrum in deuterated pH = 6.0 solution, 9.509 GHz; same conditions as in Figure 7A, except $\mathbf{B}_0$ = 3397 G, τ_{12} = 140 ns, 10 scans, 2 K. (C) ^{2}H ENDOR spectrum in deuterated pH = 6.0 solution, 9.388 GHz; $\pi/2$ microwave pulse width, 20 ns; $\mathbf{B}_0$, 3365 G; τ_{12}, 400 ns; τ_{23}, 51.62 μs; RF pulse width, 45 μs; repetition rate, 100 Hz; samplings per data point, 30; 256 data points per spectrum, 21 scans; temperature, 2 K. (D) ^{2}H ENDOR spectrum in deuterated pH = 9 solution, same condition as in C.

pH form, less than the change in D. This suggests to us that D changes in the high-pH form because the entire Fe−F unit shifts slightly as a unit toward the plane of heme pyrrole nitrogens. This would reduce the difference between parallel and perpendicular "crystal fields" and thereby decrease the axial orbital splitting, $\delta\epsilon_t$, by strengthening the "perpendicular" field.

^{1,2}H ENDOR and the N(ϵ)−H···F Hydrogen Bond. ^{1,2}H ENDOR has been used to identify the protonation/deprotonation site that influences the ^{19}F ENDOR. Figure 6A shows the g = 2 ^{1}H X-band pulsed ENDOR spectrum of the low-pH form of MbF in H_2O. It exhibits a sharp multiline pattern of hyperfine-split doublets centered at ν(H). Most of these transitions have been observed and assigned previously by Mulks *et al.* for sperm whale MbF, which shares a very similar heme active-site structure with MbF from horse heart.[24] In particular, an exchangeable proton that has a coupling constant of about 1.2 MHz and is assigned to the N(δ) proton of the proximal histidine

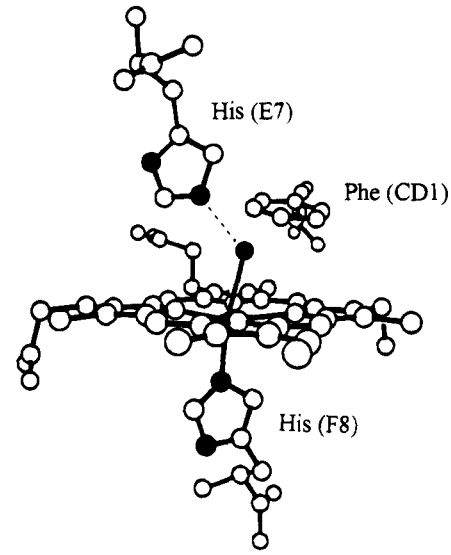

Figure 7. Illustration of the heme active site of MbF as obtained from the published structure of horse heart myoglobin[24,25] with labeled distal histidine (E7). Dotted line represents the hydrogen-bond betweeen the fluoride ligand to the N(ϵ) of distal histidine.

ligand[24] also is seen here (Figure 6, part A vs part B). In addition, we find that MbF in H_2O gives a broad ^{1}H doublet (Figure 6A) that was not seen previously and has a coupling constant A = 3.8(2) MHz. This proton also is exchangeable, as shown by its loss when MbF is in D_2O buffer (Figure 6B). The ^{2}H pulsed ENDOR spectrum taken at $g = 2$ shows a corresponding resonance with the coupling of $A(^{2}H) = 0.60(3)$ MHz as expected ($|\nu(^{1}H)/\nu(^{2}H)| = |A(^{1}H)/A(^{2}H)| = 6.51$, Figure 6C), confirming the assignment as an exchangeable proton. For comparison, the H_2O bound to high-spin Fe^{3+} of aquometmyoglobin shows a broad ^{1}H doublet at $g = 2$ with $A(^{1}H) \approx 6$ MHz.[24]

On the basis of the X-ray crystal structure of horse heart aquometmyoglobin[25,26] (Figure 7), the only exchangeable proton close enough to the heme to account for the A = 3.8 MHz signal is the N(ϵ)−H proton of the distal histidine (E7). This is well-placed to form a hydrogen bond to the fluoride ligand, similar to the hydrogen bond by which the distal histidine (E7) in sperm whale oxymyoglobin stabilizes bound molecular oxygen. As revealed by neutron diffraction analysis, the O···D distance in oxymyoglobin is 1.98 (±0.18) Å.[2] We now show that analysis of the ENDOR result confirms the presence of a N(ϵ)−H···F hydrogen bond in MbF and yields quite precise metrical parameters for it.

The 3.8(2) MHz hyperfine coupling of the distal histidine N(ϵ)−H exchangeable proton in MbF must arise from dipolar coupling to the high-spin Fe^{3+} ion,[27] as does the larger hyperfine coupling to the proton of water bound to Fe^{3+} in aquometmyoglobin.[24] The ^{1}H hyperfine coupling (A) observed at $g = 2$ is given by the expression

$$A = g_e\beta_e g_N\beta_N(3\cos^2\theta - 1)/R^3 \qquad (5)$$

where θ is the angle between the ZFS z axis and the Fe−H vector and R is the length of the Fe−H vector, as defined as

(24) Mulks, C. F.; Scholes, C. P.; Dickinson, L. C.; Lapidot, A. *J. Am. Chem. Soc.* **1979**, *101*, 1645.

(25) Evans, S. V.; Brayer, G. D. *J. Biol. Chem.* **1987**, *263*, 4263.

(26) Evans, S. V.; Brayer, G. D. *J. Mol. Biol.* **1990**, *213*, 885.

(27) The contribution from the small spin density on F^- is further reduced by a factor of $2S = 5$, as in the denominator of eq 3, and can be ignored.

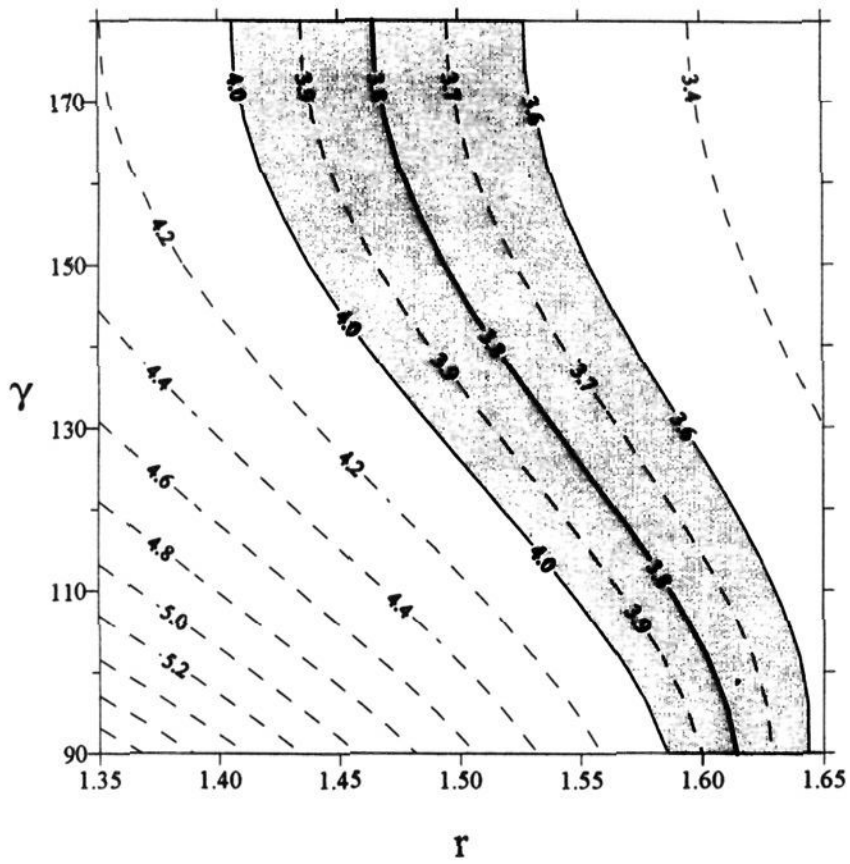

Figure 8. A contour plot of ^{1}H hyperfine coupling for the possible geometry of the H···F hydrogen-bond calculated with eq 5 using metrical parameters defined in the text. Shaded area represents the region of possible geometries based on a measured ^{1}H hyperfine coupling at $g = 2$ of $A = 3.8(2)$ MHz and $d = 2.0$ Å.

follows.[28]

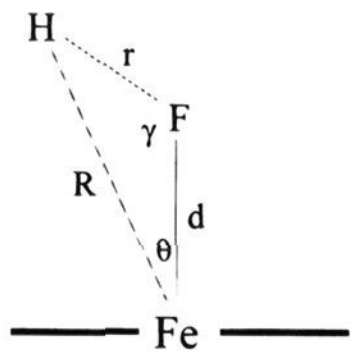

A full determination of the dipole interaction tensor for this proton would permit determination of the two parameters that fix the position of the H. However, this was not possible because of poor resolution at fields away from $g_{||} = 2$. Nonetheless, the data places tight geometric restrictions on the Fe−F···H geometry, thereby establishing and characterizing the N(ϵ)−H···F hydrogen bond.

By fixing the Fe−F bond length, one can calculate the dipolar coupling at $g_{||}$ (eq 5) as a function of the Fe−F···H angle, γ, and the F···H hydrogen bond distance, r. A contour plot of $A(\gamma,r)$ for an assumed value of $d = 2.0$ Å[19] (Figure 8) shows that, for $A = 3.8(2)$ MHz and physically possible angles of say $\gamma > 100°$, the distance must be $r < 1.64$ Å, corresponding to a rather short H-bond; the analysis gives a lower bound of $r = 1.42$ Å for $\gamma = 180°$. Thus, if one takes into consideration the uncertainties in A, for $d = 2.0$ Å, the F···H distance must lie in the range $1.42 < r < 1.64$ Å; if one further allows the range $1.95 \leq d \leq 2.05$ Å, then the maximum allowed range of distances increases, $1.35 \leq r \leq 1.66$ Å. Examination of the crystal structure of aquometmyoglobin[25,26] suggests a likely value of $\gamma \sim 120°$, in which case $A = 3.8(2)$ MHz and $d = 2.00(5)$ Å corresponds to $r = 1.57(5)$ Å. In the X-ray crystal structure of the fluoride derivative of *Aplysia limacina* myoglobin, which has a distal arginine (Arg66 (E10)), rather than a histidine residue, hydrogen bonds were found between the fluoride ion and the arginine guanidinium N−H.[29] Combining the observed N···F distance of 2.7 Å with a standard N−H bond distance of 1.05 Å gives a H···F hydrogen bond length of 1.65 Å for *Aplysia limacina* MbF, in excellent agreement with our ENDOR determination. These short H-bonds would be expected to greatly stabilize the bound fluoride, and this is corroborated by our study of sperm whale Mb mutants: fluoride does not bind to the heme if the distal heme pocket lacks a residue that can form an H···F hydrogen bond.[30]

To examine the pH dependence of the H-bond from the distal histidine residue, we collected ^{1}H and ^{2}H ENDOR spectra of MbF at $g = 2$ in both aqueous and deuterated solutions from pH 5.5 to 11. Figure 6C,D shows ^{2}H ENDOR spectra of MbF in pH = 6 and pH = 9 D_2O buffer solutions taken at $g = 2$. The exchangeable N(ϵ)−H proton is present in *both* low- and high-pH solutions, rather than being titrated away with the $pK_a = 7.6(1)$ detected in the ^{19}F ENDOR. Thus it appears that the hydrogen bond between the distal histidine and fluoride ligand remains intact even at high pH. The obvious conclusion is that the observed transformation with pH from l to h forms as seen in ^{19}F ENDOR is associated with titration of the N(δ) proton of distal histidine

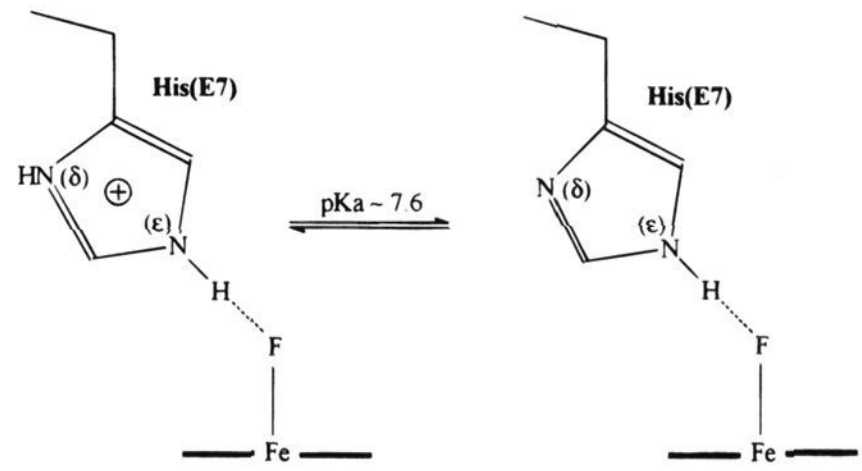

and that this indirectly influences the ^{19}F ENDOR signals through the N(ϵ)−H···F hydrogen bond. Overall, the inferred geometry and the pH transition favor our discussion of the distal-pocket interactions in terms of H-bond donation from imidazole to a fluoride ion bound to Fe, rather than as H−F bound to Fe, which has been proposed for fluoride-inhibited cytochrome *c* peroxidase.[26]

^{14}N ENDOR. The ^{14}N ENDOR spectra of MbF taken at $g = 2$ show no apparent change in either heme or proximal histidine ^{14}N transitions in the pH range studied (data not shown). This is in agreement with the ^{19}F results in that deprotonating N(δ) of the distal His(E7) has only small effects on the Fe−F bond, and further causes no measurable effects on the heme and proximal histidine (F8) nitrogens. It supports the above suggestion that the F−Fe−N(F8) may move as a unit, relative to the heme, as the distal His N(δ) is deprotonated.

Summary

The results reported here show that the combination of ^{1,2}H and ^{19}F ENDOR provides a high-resolution probe of the heme binding pocket. The ^{19}F hyperfine parameters (Table 1) give details of the ground-state bonding of the fluoroferriheme, showing ~4% spin density in an s−p hybrid orbital on fluorine. The pnZ effect yields high-precision information about the excited states, through measurements of the ZFS parameter, D. In the low-pH form of MbF, we detected a ^{1}H resonance, $A(^1H)$

(28) We may ignore here the small tilt, by which g_z and $A_{||}$ (^{19}F) are non-coincident.

(29) Bolognest, M.; Coda, A.; Frigerio, F.; Gatti, G.; Ascenzi, P.; Brunori, M. *J. Mol. Biol.* **1990**, *213*, 621.

(30) Fann, Y. C.; Nocek, J. M.; Chin, E.; Sligar, S. G.; Hoffman, B. M. To be published.

= 3.8(2) MHz, from the N(ϵ)−H···F hydrogen bond between the fluoride ligand and the protonated form of the imidazole (imidazolium) of the distal histidine (E7). ^{1,2}H ENDOR gives a H-bond length of r(F···H) ≈ 1.57(5) Å. The ^{19}F hyperfine tensor and the **g** tensor are not coaxial, with $A_{||}$ and $g_{||}$ subtending an angle of 5°. It is plausible to attribute this to a tilt of the Fe−F bond induced at least in part by the N(ϵ)−H···F hydrogen bond.

The His(E7) imidazolium ion deprotonates with a pK_a = 7.6(1), but the proton is lost from N(δ), leaving the N(ϵ)−H···F bond intact, with no detected changes in the ^{1}H coupling constant. This implies that there is no more than a small change in H-bond geometry. The ^{19}F hyperfine coupling, $A_\perp$(^{19}F), is slightly (~5%) larger than that of the low-pH form, the Fe−F tilt angle is slightly smaller, 3.5°, and the Fe^{3+} ion ZFS parameter, D, is ~15% less than the low-pH value of D = 6.1(1) cm^{-1}. A plausible scenario would have the change at N(δ) of His(E7) relax the distal-pocket structure, with concomitant slight motion of F−Fe−His(F8) relative to the heme plane. A surprising finding is a deuterium isotope effect on the ^{19}F coupling constant in the low-pH form, but not in the high-pH form, suggesting the loss of the N(δ)−H proton of the distal imidazolium transmits an effect to the N(ϵ)−H···F interaction.

The use of this probe to study mutations in the Mb distal pocket as well in other hemoproteins will be reported later.

Acknowledgment. We thank Drs. Peter Doan and Joshua Telser for helpful comments as well as the technical expertise of Mr. Clark Davoust. This work has been supported by the NIH (HL-51084-01, HL-13531).

JA950074O